

# 1 **Experimental Platform to Facilitate Novel Back Brace Development for the** 2 **Improvement of Spine Stability**

3 L. Cooper<sup>1</sup>, A. Gullane<sup>1</sup>, J. Harvey<sup>1</sup>, A. Hills<sup>1</sup>, M. Zemura<sup>1</sup>, J. Martindale<sup>2</sup>, A.  
4 Rennie<sup>1</sup>, D. Cheneler<sup>1</sup>

5 <sup>1</sup>*Engineering Department, Lancaster University, Lancaster, LA1 4YW, UK*

6 <sup>2</sup>*Wrightington Wigan and Leigh NHS Foundation Trust, Wigan, WN1 2NN, UK and*  
7 *Lancaster University Health Hub, Lancaster University, Lancaster, LA1 4YG, UK*

8

9 The spine or ‘back’ has many functions including supporting our body frame whilst  
10 facilitating movement, protecting the spinal cord and nerves and acting as a shock  
11 absorber. In certain instances, individuals may develop conditions that not only cause  
12 back pain but also may require additional support for the spine. Common movements  
13 such as twisting, standing and bending motions could exacerbate these conditions and  
14 intensify this pain. Back braces can be used in certain instances to constrain such  
15 motion as part of an individual’s therapy and have existed as both medical and retail  
16 products for a number of decades. Arguably, back brace designs have lacked the  
17 innovation expected in this time. Existing designs are often found to be heavy, overly  
18 rigid, indiscrete and largely uncomfortable. In order to facilitate the development of  
19 new designs of back braces capable of being optimised to constrain particular motions  
20 for specific therapies, a numerical and experimental design strategy has been devised,  
21 tested and proven for the first time. The strategy makes use of an experimental test rig  
22 in conjunction with finite element analysis simulations to investigate and quantify the  
23 effects of back braces on flexion, extension, lateral bending and torsional motions as  
24 experienced by the human trunk. This paper describes this strategy and demonstrates its  
25 effectiveness through the proposal and comparison of two novel back brace designs.

26 **Keywords:** additive manufacturing, back braces, spine, finite element analysis, medical  
27 design

## 28 ***Introduction***

29 The single largest cause of disability internationally is back pain, with lower back pain

30 having a prevalence of 9.4% globally (Hoy, et al., 2014). This has a significant economic  
31 impact with 149 million working days lost per year globally due to lower back pain (Office  
32 for National Statistics, 2017). The modern way of life is a major contributing factor, with  
33 poor posture, an aging population and a sedentary lifestyle all leading to an increased risk  
34 (Morl & Bradl, 2013) (Woolf & Pfleger, 2003). Similarly, there exists a plethora of medical  
35 conditions affecting the spine (Woolf & Pfleger, 2003).

36 Whilst some conditions benefit from free movement, others benefit from constraint to support  
37 the back and reduce pain. For instance, back braces limit the motion of the spine to stabilise  
38 weak, injured or fractured vertebrae and prevent progression of spinal deformity (Hawkinson,  
39 2016) (Kawaguchi, et al., 2002). The extent of motion restriction could be of great interest  
40 and importance. Current brace designs can reduce trunk motion sufficiently to prevent pain or  
41 further injury for the prescribed recovery time whilst allowing the wearer to carry out some  
42 thoracolumbar motion (Cholewicki, et al., 2007). Where designs fall short is in restricting  
43 specific trunk motion, i.e. restriction limited just to lateral bending, for instance. As some  
44 musculoskeletal back conditions actually benefit from movement (Longo, et al., 2012),  
45 targeted restriction, as compared to gross restriction, deserves further investigation.

46 In addition, prolonged wear of rigid back braces can lead to substantial muscle mass loss due  
47 to reliance on the brace to impede motion (Eisinger, et al., 1996). Current designs restrict  
48 muscle recruitment in brace conditions inducing further problems for the patient. Research  
49 into soft braces largely indicates no modification to abdominal and trunk muscles if the  
50 prescribed wearing period is adhered to (Fayolle-Minon & Calmels, 2008) (Cholewicki, et  
51 al., 2010). The inverse relationship that exists between the extents of muscle restriction  
52 against comfort of the brace attributes to the difficulty in gauging the effect of prolonged  
53 wear of rigid braces (Hsu, et al., 2008).

54 Two methods of measuring motion of the spine are employed in the literature and  
55 subsequently can be applied to test the effectiveness of back braces: biomechanical models  
56 (Ivancic, et al., 2002), and through electromyography (EMG) data from live healthy subjects  
57 in brace conditions (Cholewicki, et al., 2007) (Cholewicki, et al., 2010) (Lariviere, et al.,  
58 2014). Cholewicki *et al.* (Cholewicki, et al., 1995) conducted experiments on subjects in the  
59 upright standing posture position and performed near maximal ramp contraction, which is the  
60 body moving from rest to the maximum angle it can bend in flexion, extension and lateral  
61 bending, in each case checking the extent of muscle recruitment of torso muscles for spine  
62 stability. However, due to ethical issues with regards to access of patient data or use of live  
63 subjects, no current reliable methods exist to test the effectiveness of back braces. This  
64 research aims to address the shortcomings of the current design process and provide a method  
65 of assessing back braces quantifiably.

66 In this work, the design and operation of an experimental test rig for the quantified design,  
67 comparison and optimisation of back braces is described, hence providing a method for the  
68 braces to be more easily and ethically tested. The test rig incorporates an artificial spine and  
69 torso, shown here to be mechanically equivalent to a human torso. In order to prove its  
70 effectiveness, two novel back brace designs have been tested on the rig. It has been shown  
71 that by using the test rig, it is possible to quantify the reduction in flexion, extension, lateral  
72 bending and torsion.

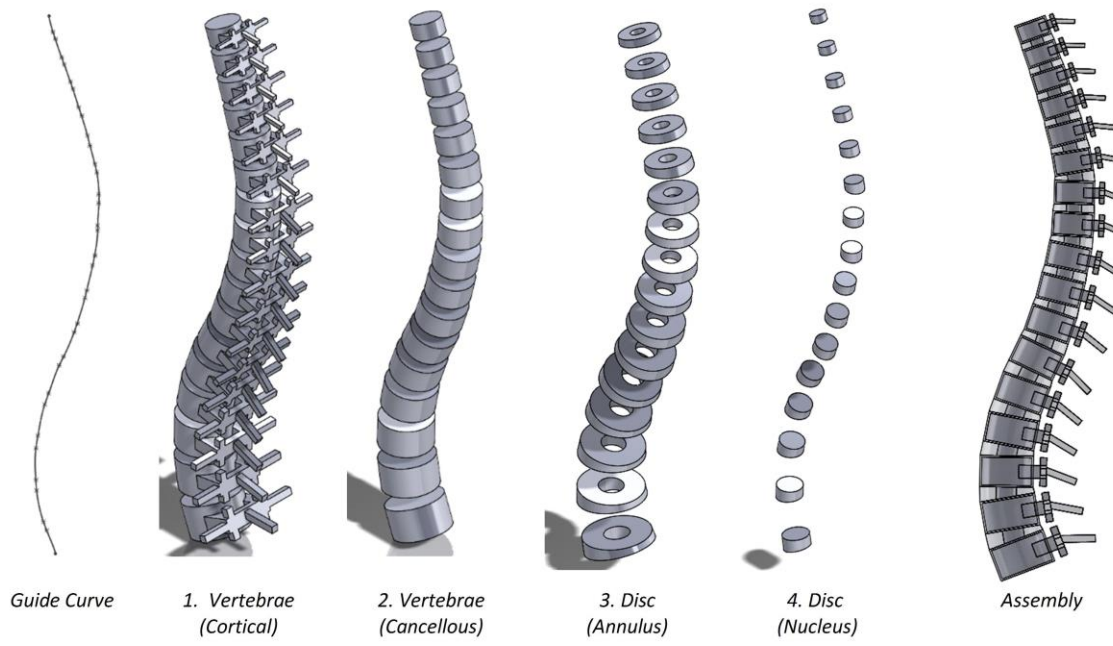
73 The test rig, including spine, torso and brace design have been modelled using finite element  
74 analysis (FEA). This analysis allows for the study of spine motion during brace development.  
75 Through comparison to studies found in the literature, the validation simulations presented  
76 show that the simplified geometry, constraints and engineering materials used here have a  
77 mechanical response similar to equivalent components found in the human torso. Many

78 complex FEA models of the spine exist, however only particular segments relevant to the  
79 area of study are usually created, hence the movement of a detailed full spine model has  
80 never been fully investigated in FEA (Huynh, et al., 2012) (Carboni & Dal Pozzo, 2017),  
81 especially with the consideration of the full torso and many of the soft tissue therein.  
82 However recent advances in complete musculoskeletal models of the human spine in  
83 multibody dynamic simulations, which could be incorporated into FEA models, should be  
84 noted (Bayoglu, et al., 2019). The spine material models employed throughout previous work  
85 varies tremendously, with the intervertebral discs often modelled as simple cylinders between  
86 spinal vertebrae (Kurutz, 2010). It is common to split the vertebrae into both cortical and  
87 cancellous bone, and the intervertebral discs into nucleus pulposus and annulus fibrosus  
88 sections. Additionally, ligaments are commonly found within FEA spine models and the  
89 muscle systems seldom modelled. Here, a FEA model of the spine and torso is described and  
90 it is shown how these simulations can facilitate back brace development.

## 91 ***Methods***

### 92 *Experimental Rig Design*

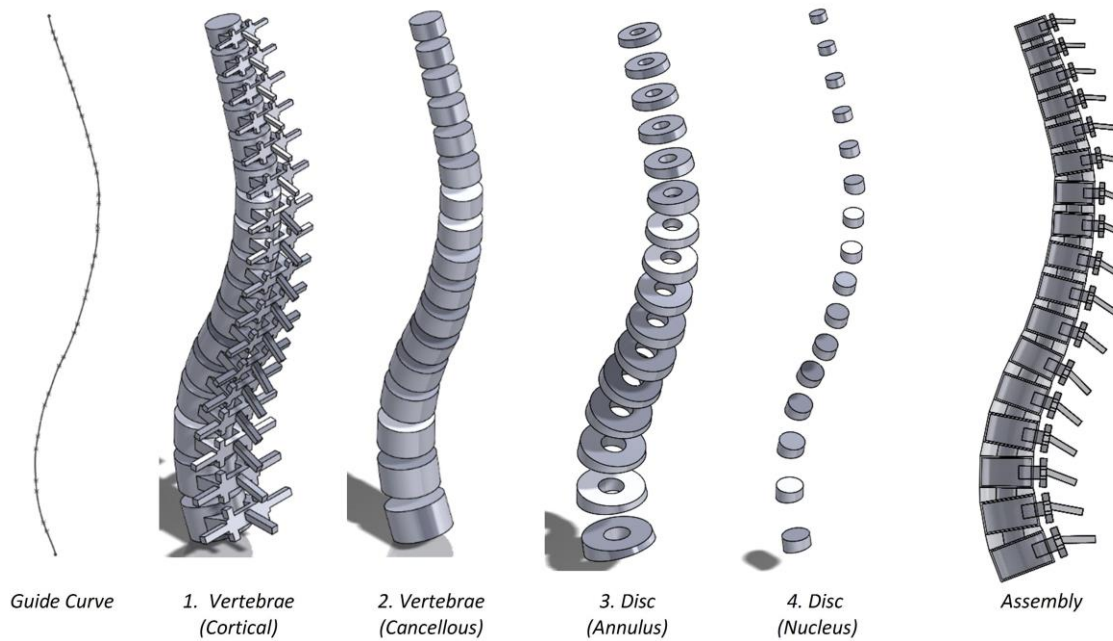
93 The artificial spine and torso used on the test rig was developed using FEA to ensure it was  
94 mechanically equivalent to a human torso. The spine geometry developed was that of an  
95 average adult male. Dimensions were found through analysing studies undertaken by Panjabi  
96 *et al.* (Panjabi, et al., 1992), who used CT scans of a cadaver to determine the curvature of the  
97 spine and quantitatively describe the surface anatomy of 60 lumbar vertebrae. A simplified  
98 computer-aided design (CAD) model, shown in



99

100 Figure 1, was then created for use within the study.

101



102

103 Figure 1 - Breakdown of parts present within the spine CAD model

104 The CAD assembly permitted the breakdown of the spine into its constituent parts, which

105 allowed separate material models to be applied to each. The Mooney-Rivlin two-parameter

106 model was chosen to represent the discs, a model which predicts the behaviour of

107 hyperelastic materials through curve fitting to data and used in numerous past studies  
 108 (Gómez, et al., 2017) (Wagnac, et al., 2011) (Schmidt, et al., 2006) (Dreischarf, et al., 2014).  
 109 The elastic modulus of vertebrae ranges from 1.5 to 3 GPa (Swamy, 2014), and so ABS1400  
 110 with an Young's modulus of 1.68 GPa (Ultimaker, 2017) was selected to represent bone  
 111 within the spine structure. Ligaments were modelled as tension-only springs and defined  
 112 through a particular stiffness (Pitzer, et al., 2016). Compressive testing of flexible  
 113 polyurethane foam samples yielded an elastic modulus of 0.128 MPa, within the limits stated  
 114 by Bonnaire *et al.* (Bonnaire, et al., 2014) for the human abdomen (0.01 to 1 MPa). Due to  
 115 the suitable elastic modulus, low cost and ease of use, it was selected to represent body mass  
 116 and soft tissue within the test rig torso.

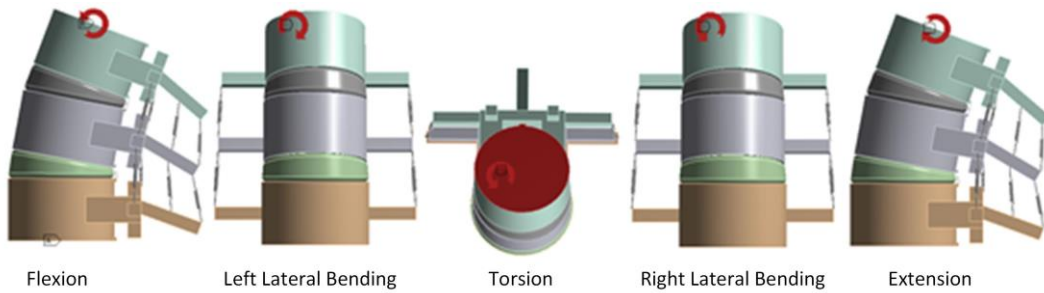
117 Table 1 provides a breakdown of the material properties.

118 Table 1 - Material property data

Part	Material Model	Modulus [MPa]	Poisson's Ratio $\nu$	Reference
<b>Accurate Model</b>				
Cortical Bone	Linear Isotropic	5000	0.3	(Rohlmann, et al., 2006)
Cancellous Bone	Linear Isotropic	10	0.2	(Kurutz, 2010)
Annulus Fibrosus	Mooney-Rivlin	C1=0.14, C10=0.56, D=0.143		(Gómez, et al., 2017)
Nucleus Pulposus	Mooney-Rivlin	C1=0.03, C10=0.12, D=0.067		(Gómez, et al., 2017)
Ligaments	Spring Elements			(Pitzer, et al., 2016)
<b>Test Rig</b>				
ABS1400 (Vertebrae)	Linear Isotropic	1681.5	0.3	(Ultimaker, 2017)
Soft Polyurethane Foam (Torso)	Linear Isotropic	0.128	0.3	
Hard Polyurethane Foam (Discs)	Linear Isotropic	5	0.3	(Seo, et al., 2013)

119  
 120 In order to benchmark the effect of the geometry and constraints in the artificial spine model  
 121 used here against that of an actual human spine, the maximum displacement of the L2, L3  
 122 and L4 vertebrae were examined using the mechanical properties of human tissue and

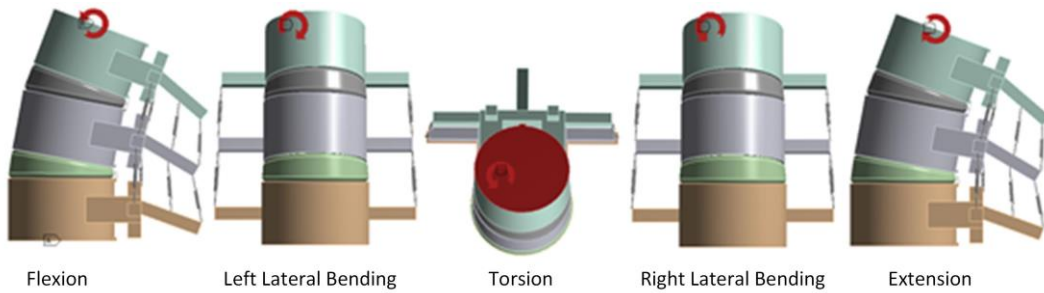
123 compared against studies undertaken by Wang *et al.* (Wang, et al., 2006). In that study, and  
 124 replicated here, a moment of 10 Nm was applied upon the superior surface of the L2 body,  
 125 and the inferior surface of the L4 body was fixed. This is the maximum load that the spine  
 126 can withstand before any spinal injury is caused (Yamamoto, et al., 1989). Each loading  
 127 condition is displayed in



128 Flexion Left Lateral Bending Torsion Right Lateral Bending Extension **Figure 2**

129 and the comparative results given in Table 2. The data shows that there is a reasonable  
 130 equivalency in the mechanical response between the geometry and constraints used in the  
 131 spine model here and those found in an actual human spine.

132



133 Flexion Left Lateral Bending Torsion Right Lateral Bending Extension **Figure 2**

134 - L2-L3-L4 Loading and boundary conditions

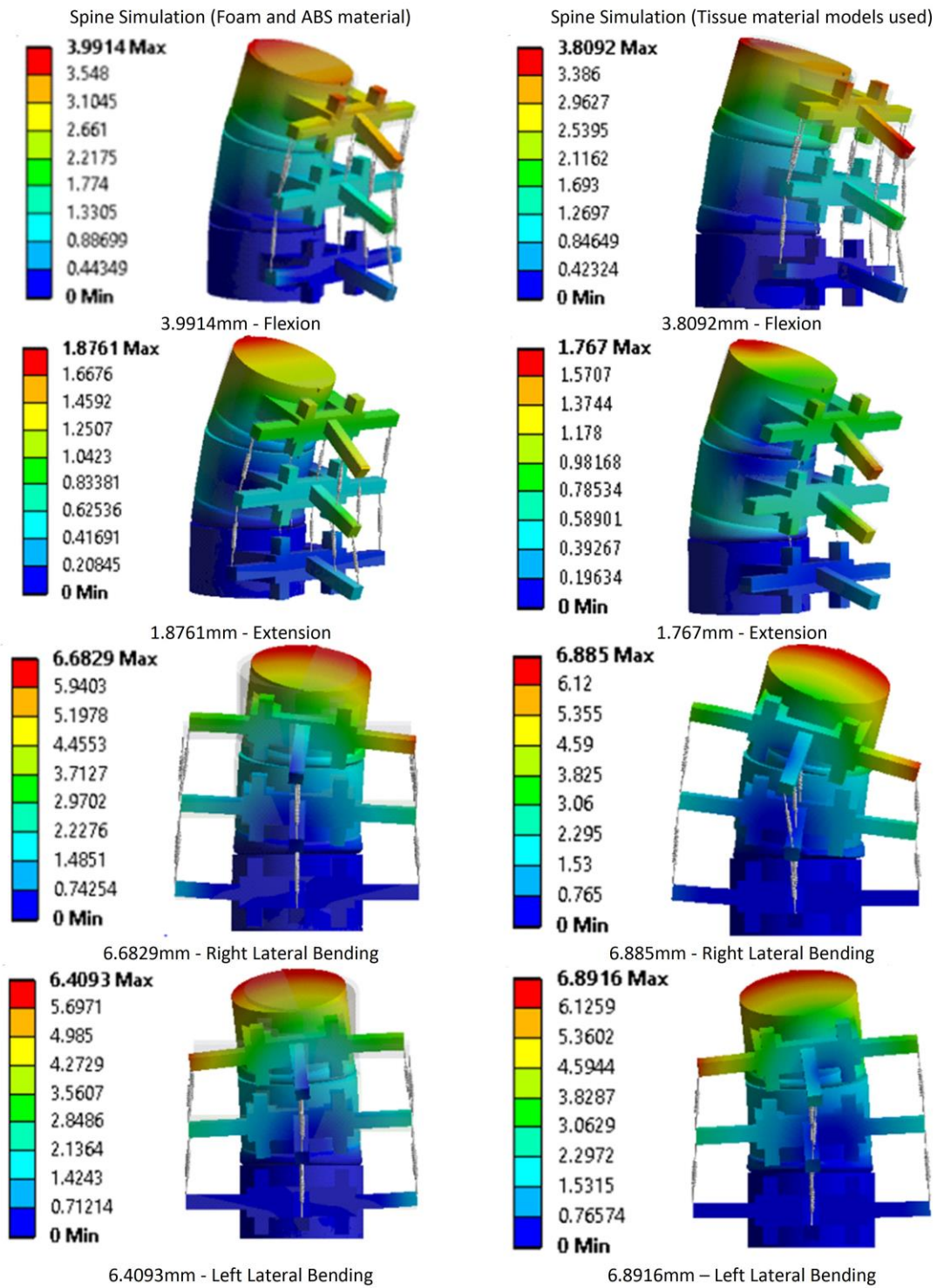
135 Table 2 - Simulation 2 results summary

	<b>Flexion</b>	<b>Extension</b>	<b>Left Bending</b>	<b>Right Bending</b>
<b>L3 Displacement (mm)</b>	1.8272	1.263	2.8389	2.8355
<b>Literature Value (mm) (Wang, et al., 2006)</b>	1.66	0.97	3.27	3.27

136

137 Given this data, it can be seen that even with the simpler geometry used within the test rig,

138 the spine is still undergoing equivalent motion. To ensure the engineering materials used in  
139 the test rig are suitable, the materials properties in the simulation were changed to that of  
140 ABS and polyurethane foam, as used in the test rig. The data was compared to the model  
141 previously described, which used the properties of human tissue so that it could be verified  
142 that the materials being used were mechanically equivalent. A close match is seen in Figure  
143 3, highlighting how the materials and geometries used within the test rig are a suitable choice.  
144 Again, the springs shown represent the tension-only spring elements that model the  
145 ligaments.  
146



147

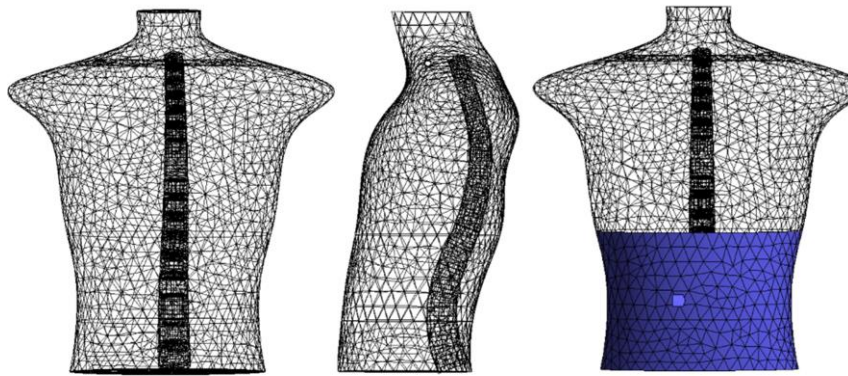
148 Figure 3 - Total L2-L3-L4 displacement comparisons

149

150 To investigate the mechanical behaviour of the full torso, the spine was added to a torso CAD

151 model. Multiple cross-sectional dimensions were taken from a human torso mannequin to

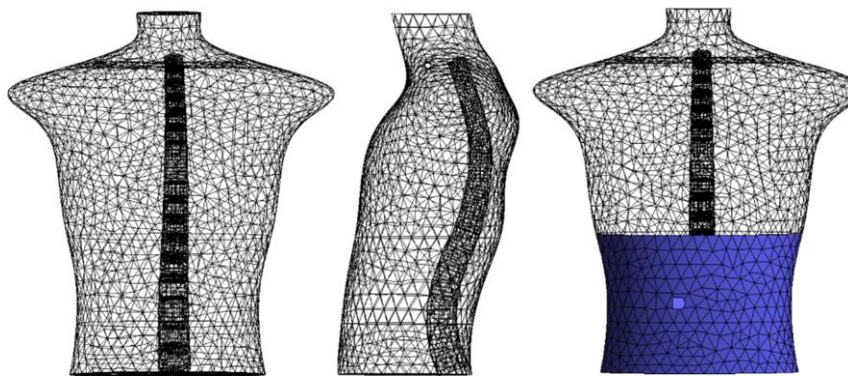
152 achieve the required external geometry, as shown in



153

154 Figure 4.

155

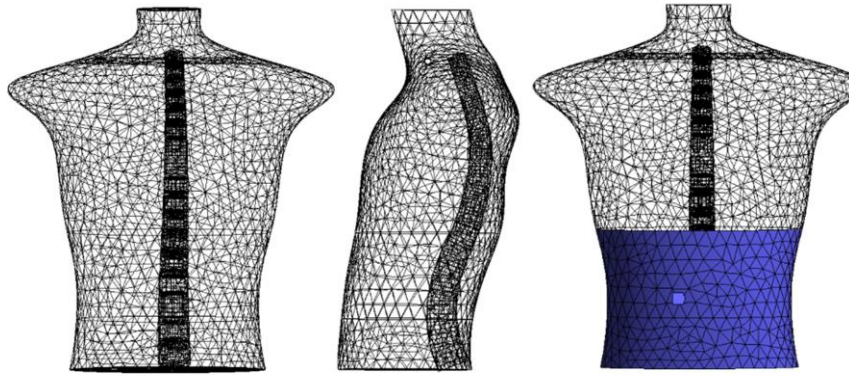


156

157 Figure 4 - Torso and spine CAD model. The figure on the right shows the position of a  
158 hypothetical back brace in blue. This was modelled as an elastic foundation for initial design  
159 purposes.

160

161 The final step for verifying the effectiveness of the simulated torso was to show how a simple  
162 back brace around the waist achieves a reduction in the range of motion.



163

164 Figure 4 shows the sectioned area where a back brace would impart a pressure on the torso.

165 The elastic support boundary condition provides a stiffness normal to the surface it is applied

166 on and is defined through a foundation stiffness. This stiffness is defined as the pressure

167 required to produce a unit of normal deflection (ANSYS, 2017) and thus is representative of

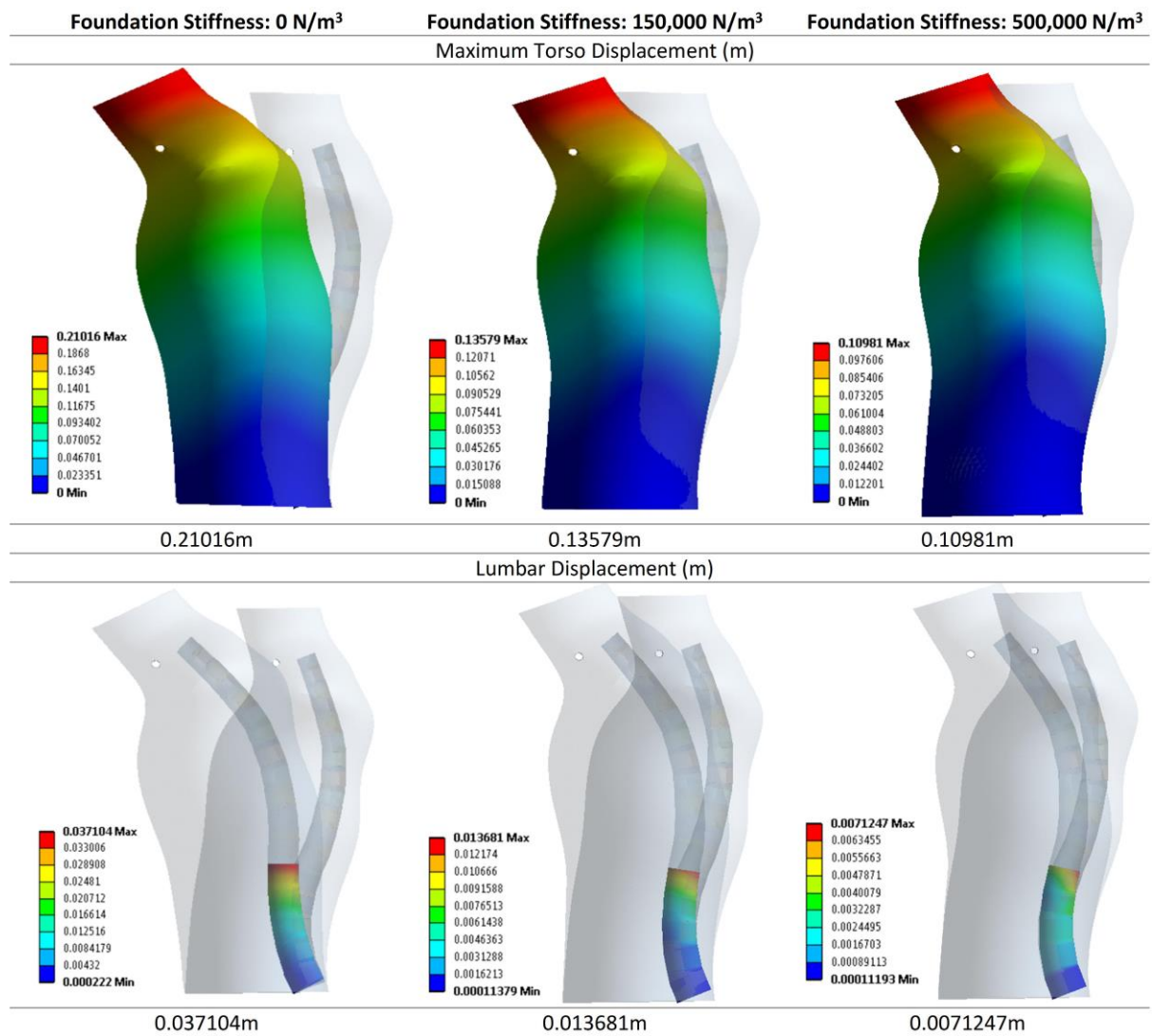
168 an elastic brace being worn.

169 A normal load of 58.4 N was applied to the sternum, to be consistent with later experiments

170 and to simulate the spine and torso displacement during flexion. Foundation stiffness was

171 incrementally increased and both maximum displacement and lumbar displacement analysed

172 (



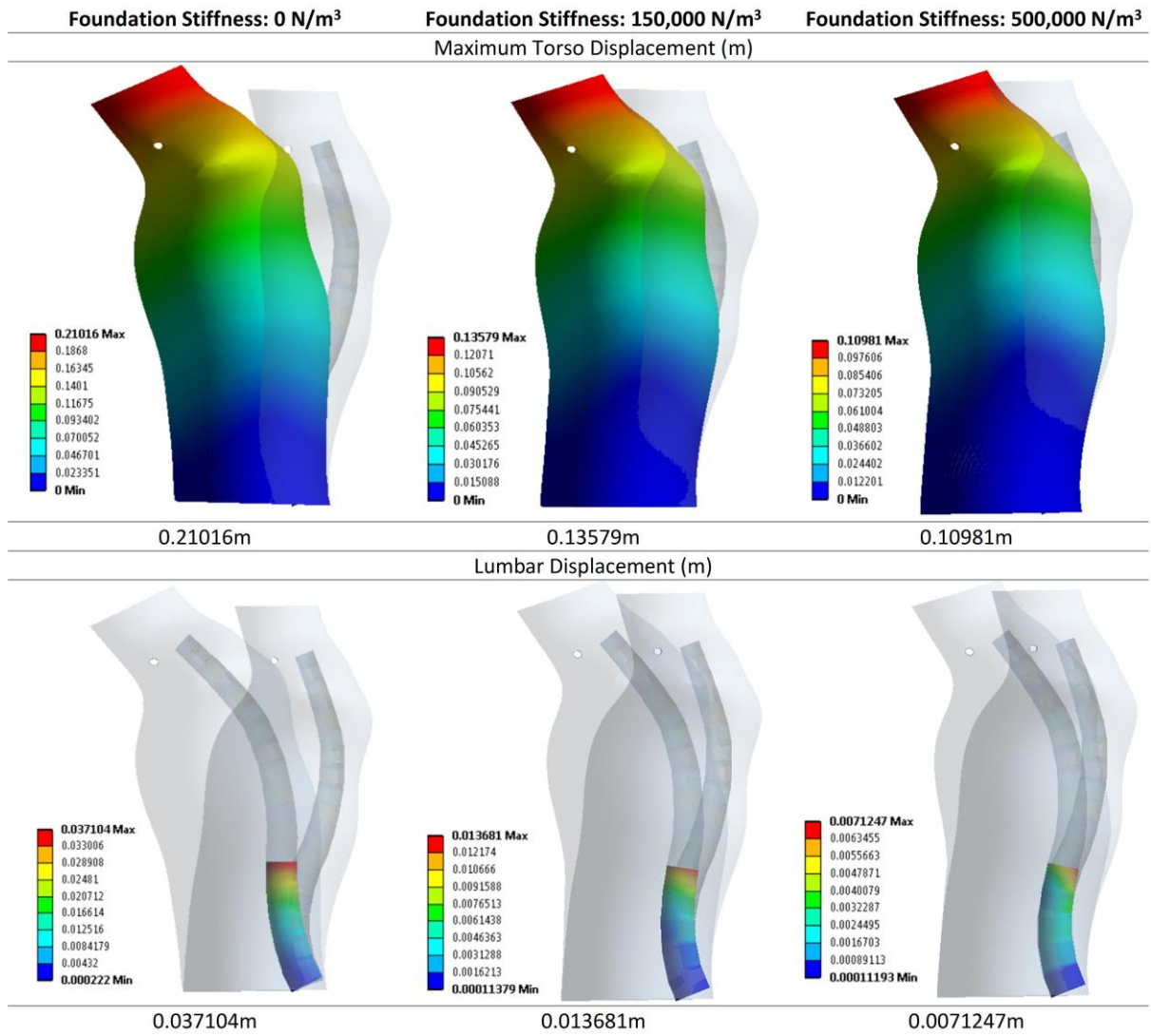
173

174 Figure 5). It can be seen that through increasing the pressure around the waist, a reduction in

175 the total displacement of the torso is possible. It is also noted that the reduction in

176 displacement is more evident in the lumbar region. It is postulated that data such as that

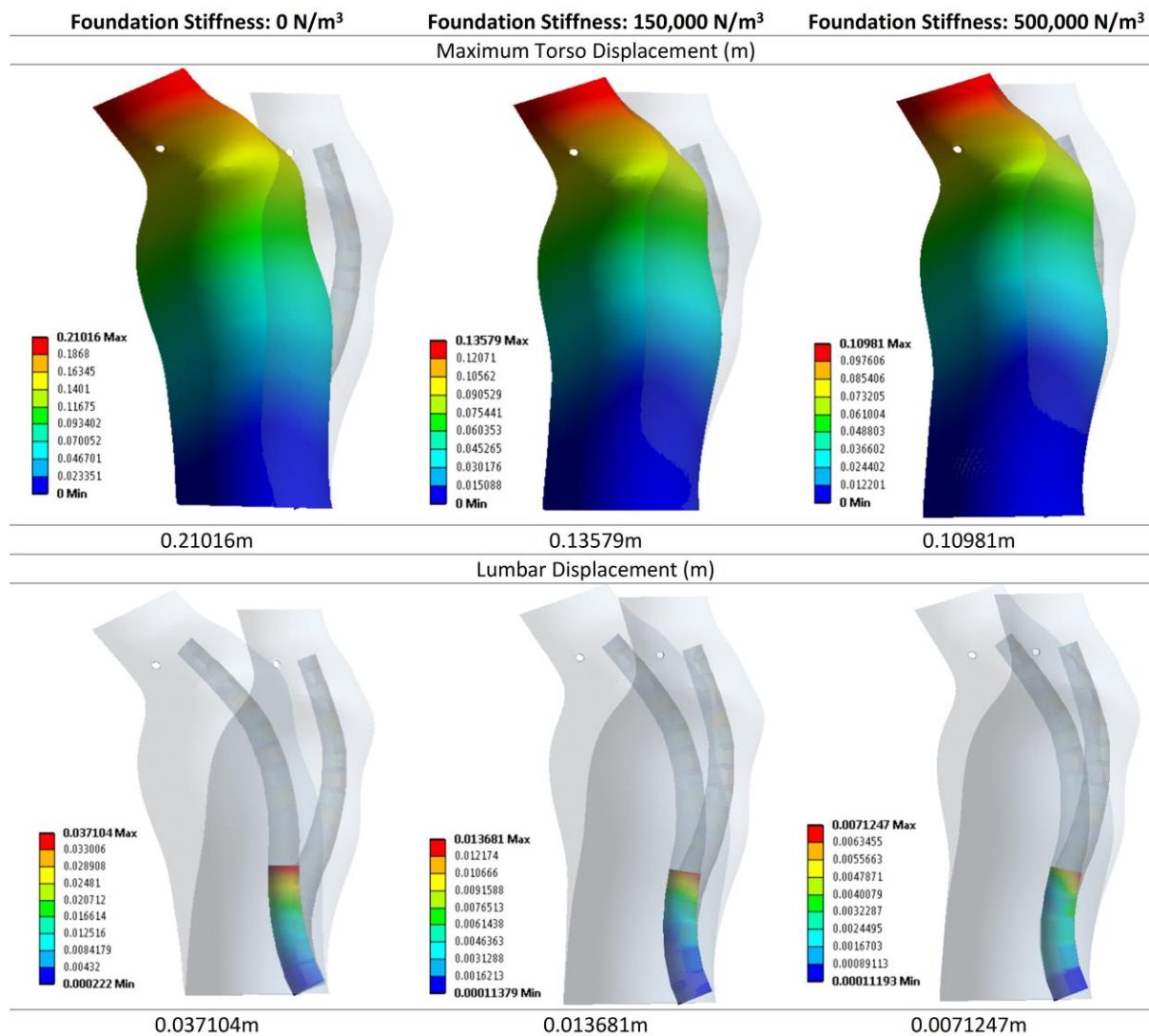
177 derived from



178

179 Figure 5 may be used to tune or design a back brace to a desired range of motion.

180



181

182 Figure 5 - Braced foam torso displacement

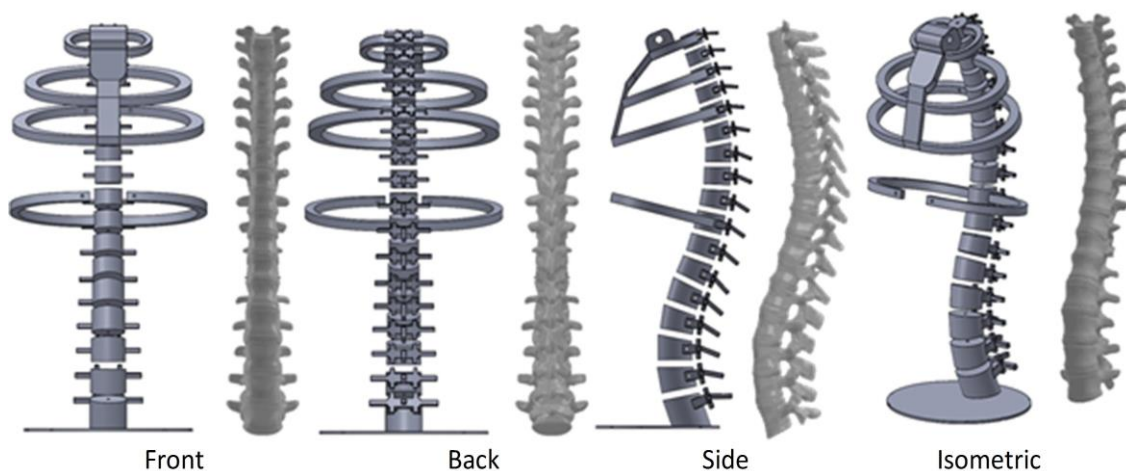
183

184 *Test Rig Fabrication*

185 The test rig comprises two fundamental features: an artificial mechanically equivalent human  
 186 torso, and a frame mechanism designed to manipulate the torso into flexion, extension, lateral  
 187 bending and torsional motions. Unlike the FEA models, the fabricated vertebrae were treated  
 188 as a single material structure to aid in manufacture. This does not affect the mechanical  
 189 behaviour of the torso. Such a structure lends itself to fused deposition modelling (FDM; an  
 190 additive manufacturing process), a method well suited to fabricating the unique geometries of  
 191 vertebrae, and hence the method adopted in this instance. All vertebrae, ribs and sternum

192 were additively manufactured using FDM on a Ultimaker 2 (Ultimaker-Geldermalsen,  
193 Netherlands) with a 0.4 mm nozzle. A 3mm diameter ABS1400 feedstock and a nozzle  
194 temperature of 240 °C was used (build plate temperature was 80 °C). All intervertebral discs  
195 were cast as one collective piece of medium density polyurethane foam (Polycraft 022-  
196 medium foam; from MB Fibreglass), in a two-part mould fabricated using FDM. This piece  
197 was then cut to the correct geometries in sections using a scalpel.

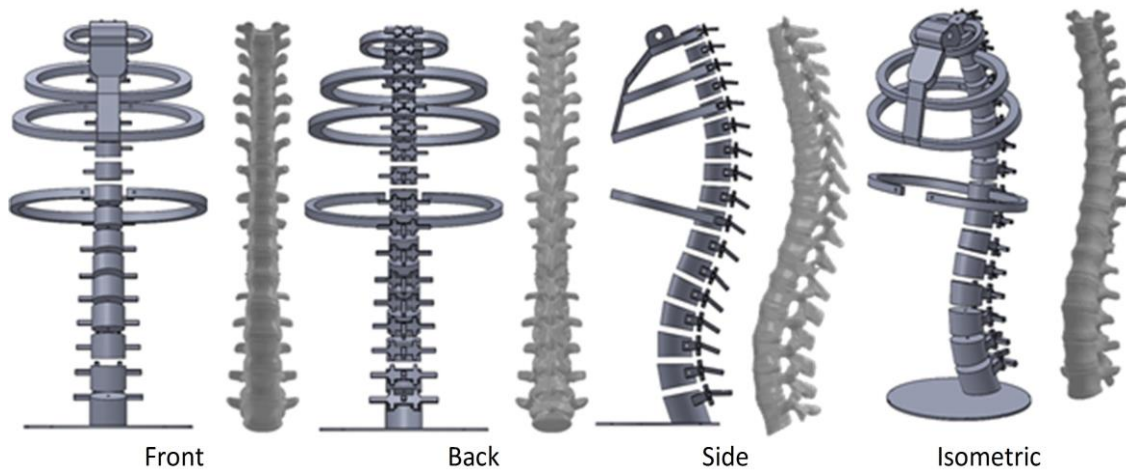
198 The ribcage contributes to a reduction in flexibility in the torso and an increase in motion  
199 stability [27]. The ribcage was designed based on cadaver data of an average male, combined  
200 with reverse engineering of existing skeletal models (Panjabi, et al., 1992). Simplifications  
201 were made to the geometry of the ribs and sternum to improve the quality of the parts  
202 produced using FDM. To further simplify the ribcage design, only essential ribs were  
203 included. These include ribs necessary for load distribution. Only four rib pairs were  
204 therefore included in the design, connected to vertebrae T1, T3, T5 and T10. The ribcage  
205 was also fabricated from ABS1400 to simulate bone within the spinal structure. The  
206 assembled CAD model of the artificial spine is shown in



207  
208 Figure 6 and compared directly to CT scan data. This CT scan data was retrieved from an  
209 open access source (An, 2014) which used Materialise Mimics software (Materialise, 2018)  
210 to convert CT slices into a solid model. Radiographic data was taken from a male cadaver

211 without any apparent spine trauma or pathological effects. The data is used here purely for  
212 visual comparison.

213

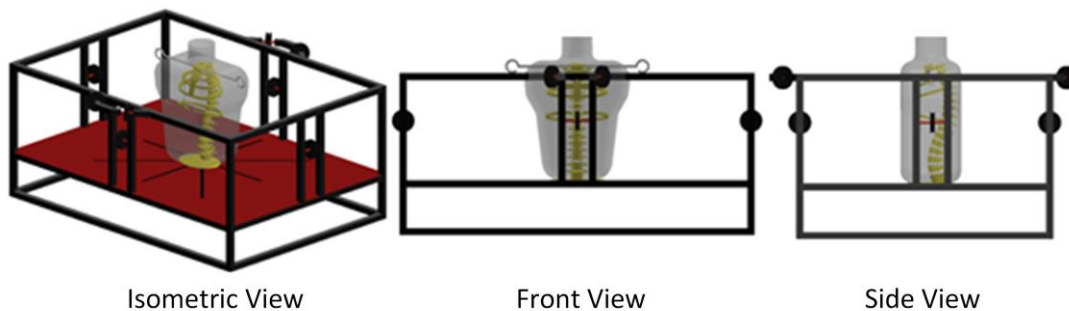


214

215 Figure 6 - Spine CAD assembly compared with CT scan data of example human spine

216

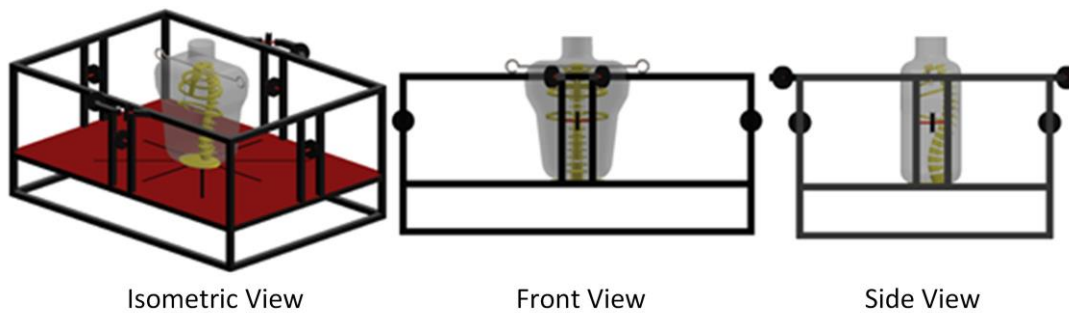
217 The test rig comprises a steel framework featuring a set of pulley systems capable of  
218 manipulating the torso (



219

220 Figure 7). A steel rod connected to the sternum and protruding from the torso acts as the  
221 shoulders and provides a connection point for the cables attached to the pulley wheels. The  
222 front/back/lateral pulley wheels are lowered in line with the upper abdominals/obliques/lower  
223 back in order to generate true anthropomorphic motion in flexion/extension/lateral bending.  
224 Since torsional motion is greatest at the top of the thoracic spine, and progressively less lower

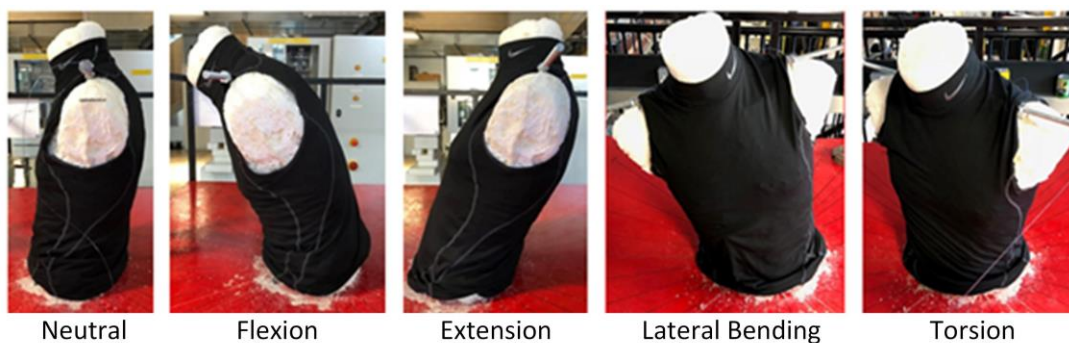
225 down the spine, the torsional motion is created in line with the T1 vertebra. The geometry of  
226 the torso was obtained by creating a mould around a torso mannequin using Plaster of Paris.



227  
228 Figure 7 - Test rig CAD assembly

229 *Test Rig Test Method*

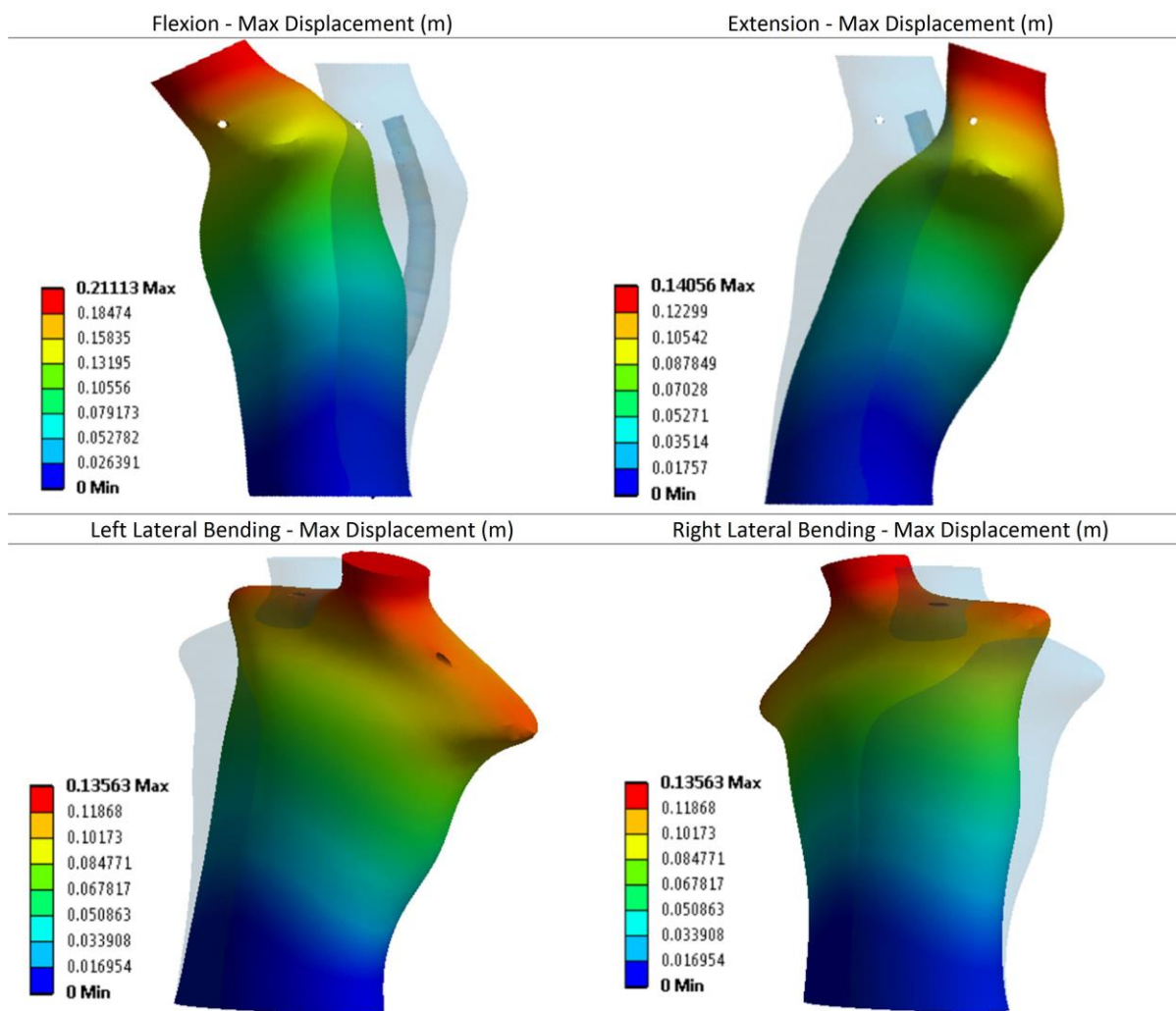
230 The intention of the test rig is to quantify and compare the reduction in motion caused by the  
231 presence of various brace designs. Three methods were used to record respective motion  
232 displacement: flex sensors attached along the centre of the torso recording bend angle of the  
233 torso; image analysis of photographs taken from fixed locations both before and after  
234 applying load (see



235  
236 Figure 8); and manual measurement of the displacement of a fixed point on the shoulder rod  
237 from the horizontal plane.

238 All three methods were used in recording flexion/extension/lateral bending; however, torsion  
239 does not lend itself to use of flex sensors or manual displacement measurement, and hence

240 relies solely on imaging. A preliminary range of motion test was undertaken on the rig and  
 241 validated using the FEA (see



242  
 243 Figure 9) model described above, and a summary of the key results obtained is given in Table  
 244 3. Load was applied to achieve a desired range of motion and the same applied on both the  
 245 mechanical rig and in simulations to provide the basis for fair comparisons.

246 Table 3 - Test rig range of motion results

	Flexion	Extension
Mass Applied (Kg)	5.95	3.0

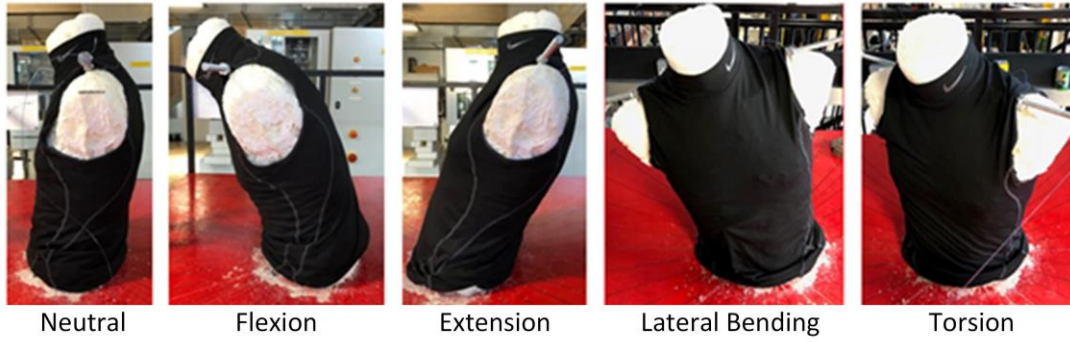


Figure 8)

Flexion - Max Displacement (m)

Extension - Max Displacement (m)

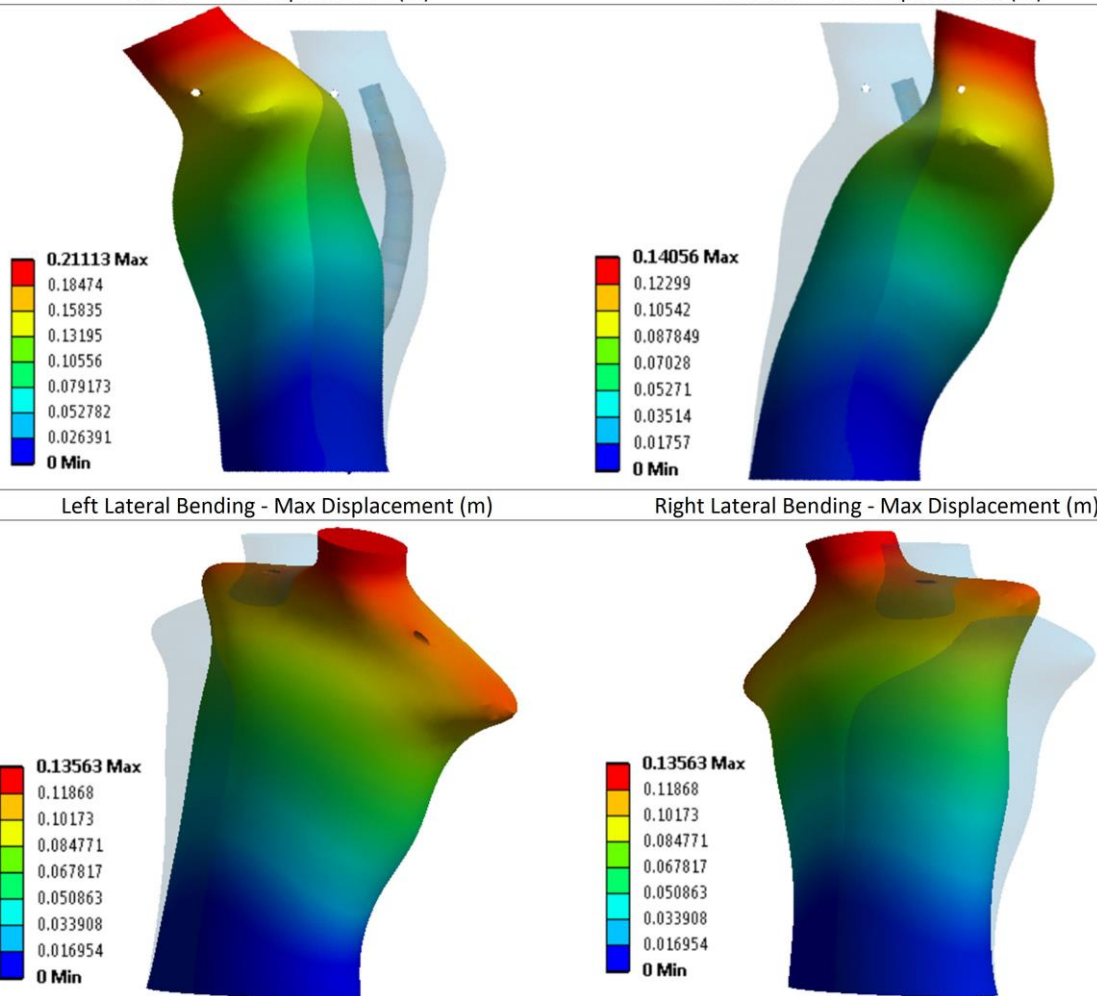
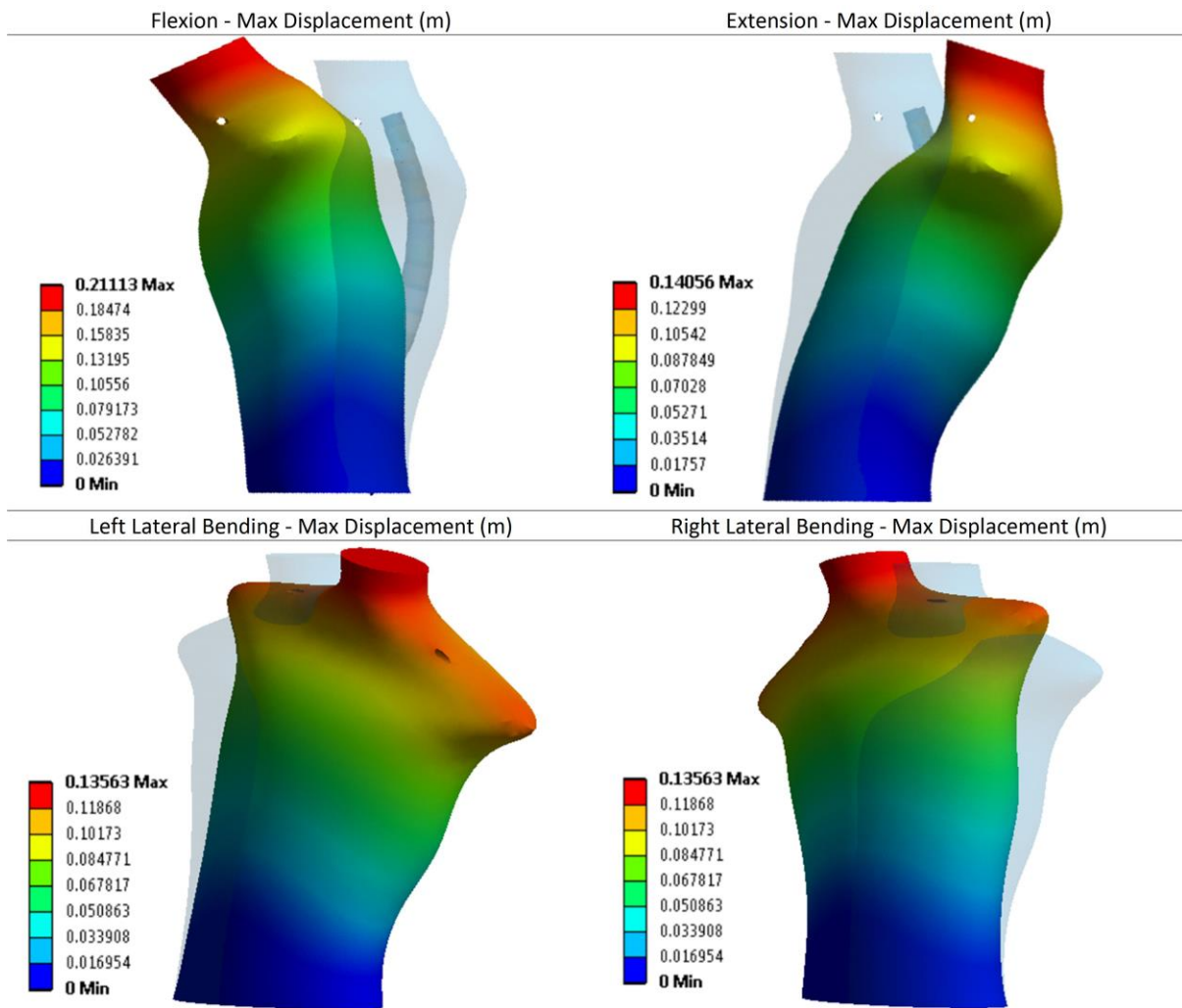


Figure 9)



248

249 Figure 8 - Test rig torso motions given loadings stated in Table 3



250

251 Figure 9 – Simulated torso displacements for comparable loadings as test rig shown in



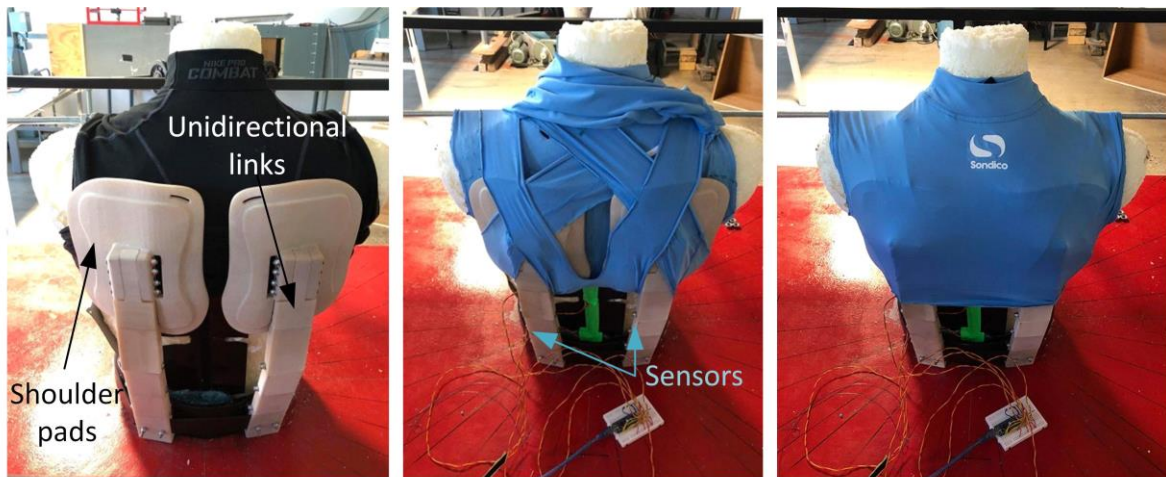
252

253 Figure 8

254 *Brace Design*

255 The first back brace design utilised a combination of topologically customised shoulder pads

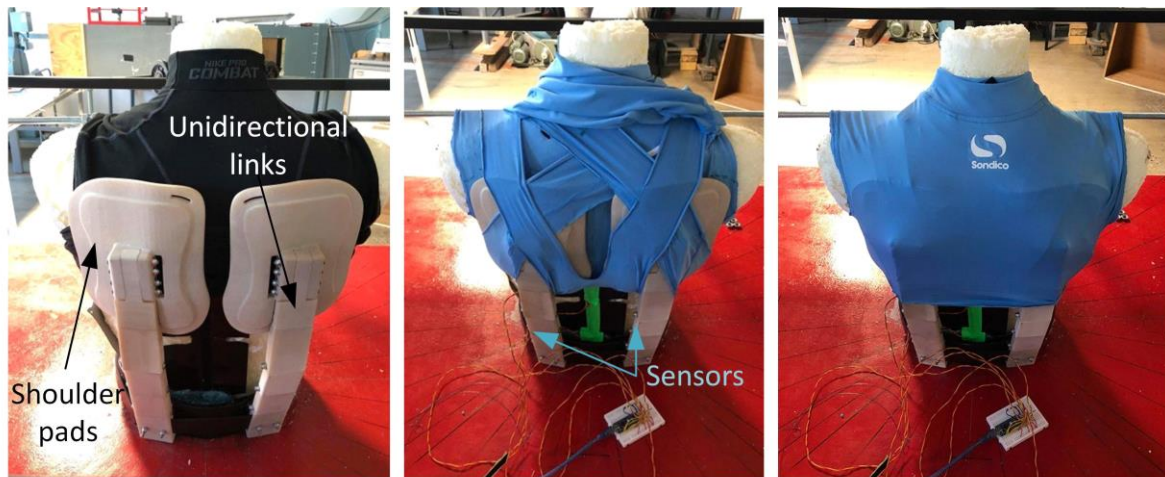
256 and unidirectional chain links (



257

258 Figure 10). The design intent of this concept was to allow flexion while restricting extension,

259 lateral bending and torsion to a noticeable degree.

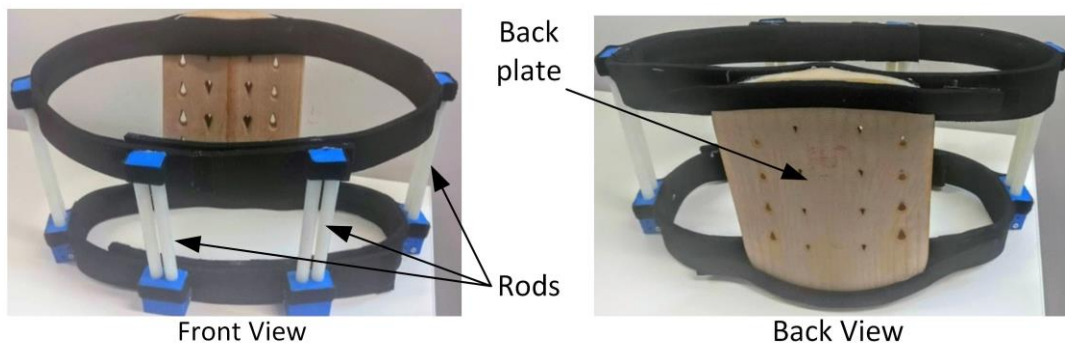


260

261 Figure 10 - Assembled 'unidirectional' linked back brace at various stages of attachment

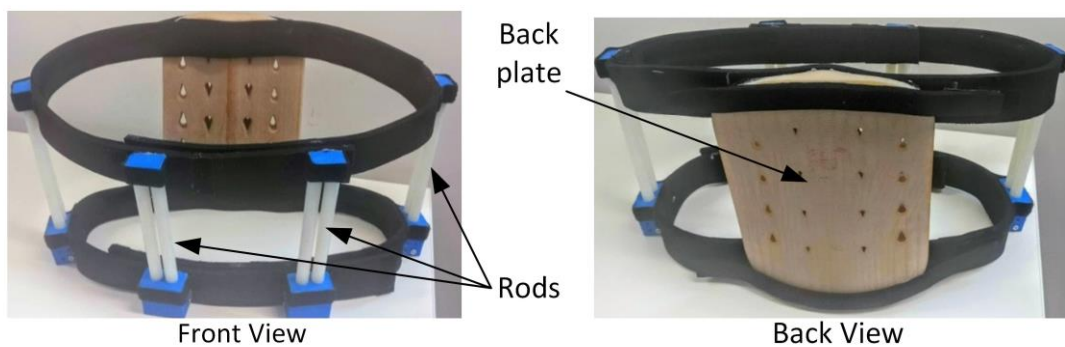
262

263 The second design combined the use of a back plate and rods (



264

265 Figure 11). The design intent of this concept was to bridge the gap between the flexible and  
 266 rigid braces currently available and to restrict flexion, extension and lateral bending in  
 267 thoracolumbar motion.



268

269 Figure 11 - Assembled combined plate and rod back brace

270 ***Test Rig Results***

271 The test rig was used to compare the behaviour of the torso when restricted using back braces  
272 and to quantifiably compare back brace design. The two novel designs (rodded and linked)  
273 were compared to two commercially available back braces, i.e. a leather weightlifting  
274 belt (Gold’s Gym) and an lumbar support brace, a back belt with metal splints (TONUS  
275 0012-01 LUX, Tonus Elast). The four braces tested are shown in



276 No Brace Weightlifting Belt Rod Brace Existing Brace Linked Brace

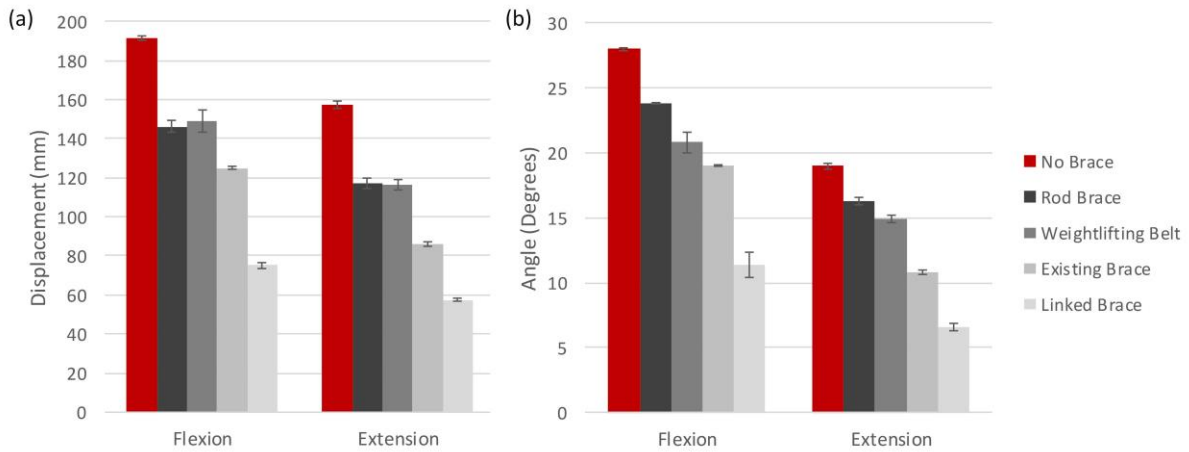
277 Figure 12, along with the control (no brace).



278 No Brace Weightlifting Belt Rod Brace Existing Brace Linked Brace

279 Figure 12 - Overview of brace conditions tested on the rig

280 *Flexion and Extension*



281

282

Figure 13 shows how in flexion, the linked brace is by far the most restrictive and the rod

283

brace the least. As expected, the displacement results show a similar pattern to the measured

284

angles. One noticeable difference between the displacement and angle data is the reduction in

285

flexion for the weightlifting belt – the displacement data shows the belt as restricting flexion

286

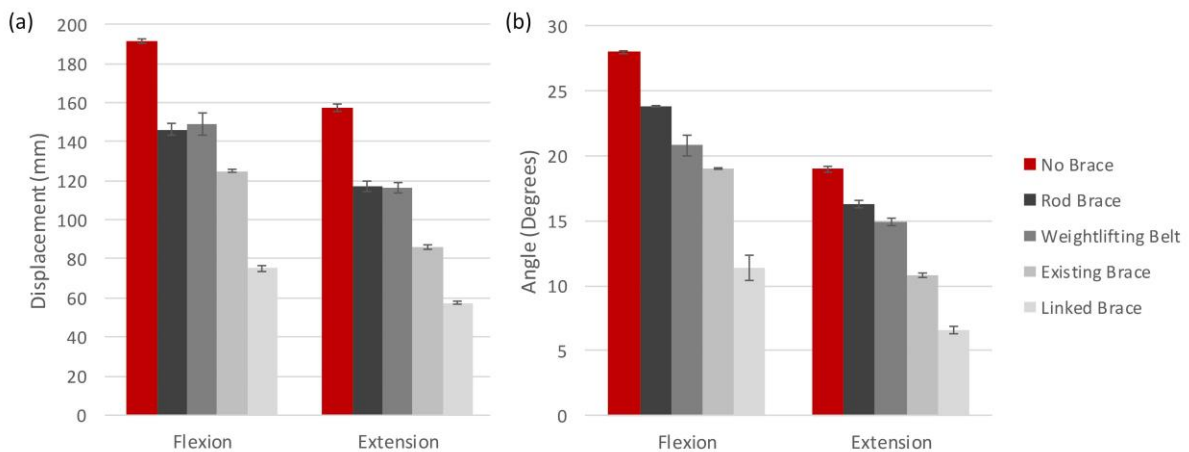
by less than the rodDED brace, whilst the angle data shows more reduction. The difference in

287

final angle between the weightlifting belt and the rodDED brace could be indicative of a shift

288

in the centre of rotation.



289

290

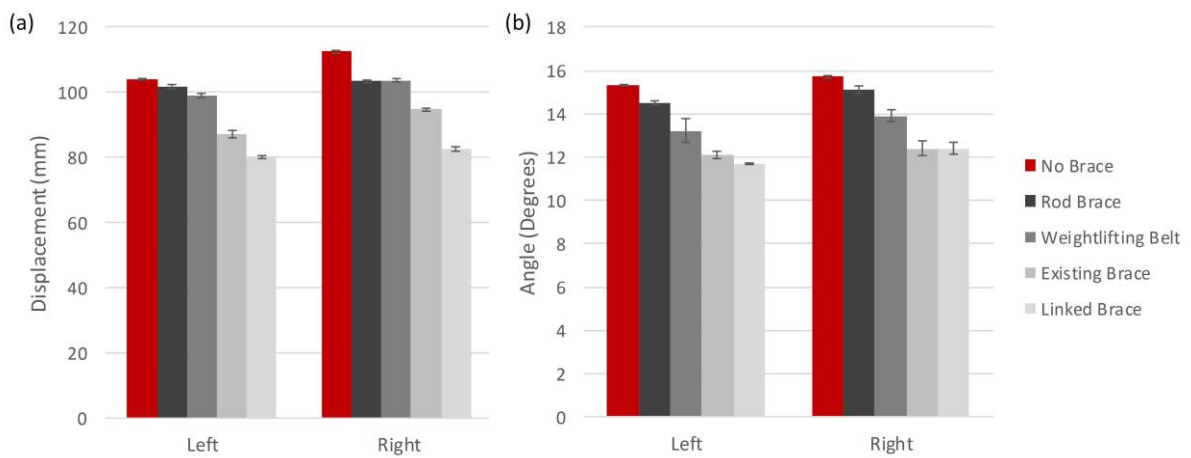
Figure 13 - Comparison of brace motion in flexion and extension. (a) Shows maximum

291

deflection, (b) shows angle of tilt

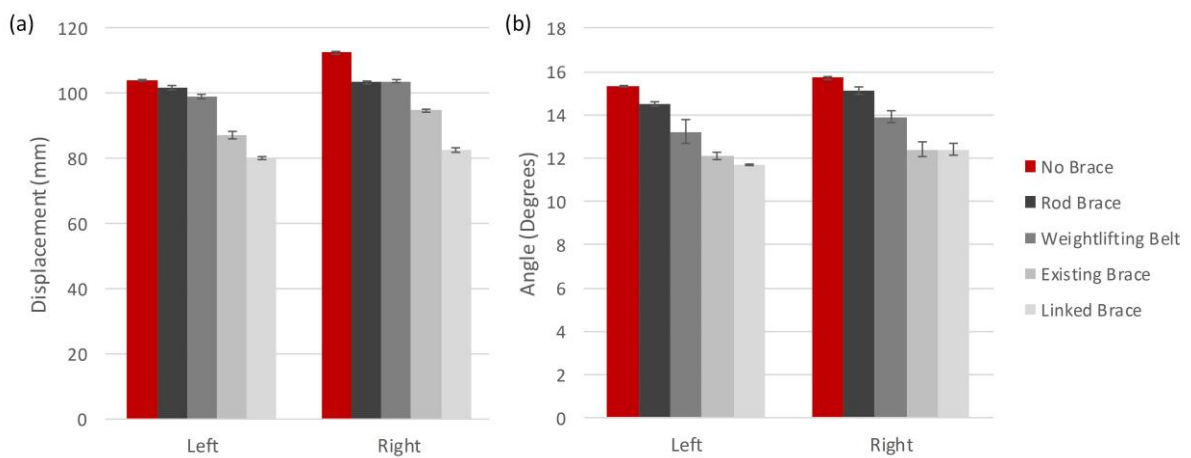
292 *Lateral Bending*

293 In both cases, lateral bending shows a discrepancy between left and right motion (



294

295 Figure 14). This may be due to inhomogeneous properties of the cast foam in the torso. Of  
296 the two designed braces, the rod brace can be seen to restrict the least motion and the linked  
297 brace the most.

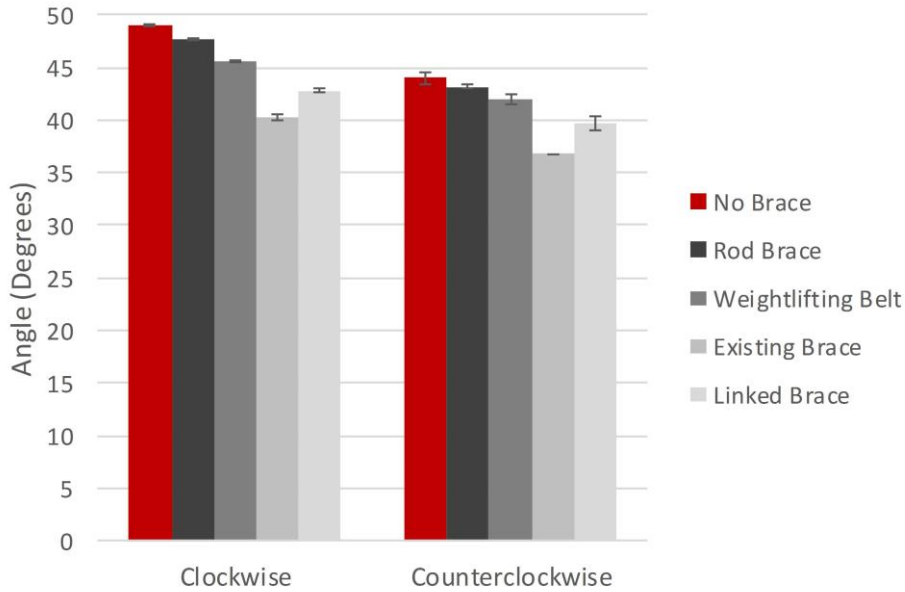


298

299 Figure 14 - Comparison of brace motion in lateral bending in both left and right directions.  
300 (a) Shows maximum deflection, (b) shows angle of tilt

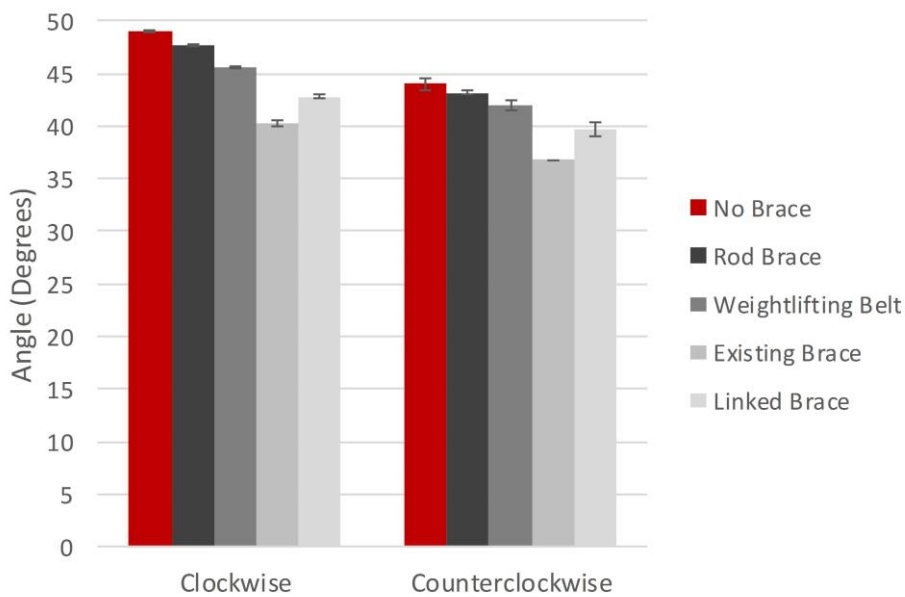
301 *Torsion*

302 From the outset of this work, it was suspected that torsion would be the most difficult motion  
303 to restrict and this has been shown to be true from the results gained. The two designed  
304 braces were less effective at reducing torsion, as evidenced in



305

306 Figure 15. The commercial elastic brace is seen to reduce the most motion, likely due to the  
 307 larger contact area with the body of the torso.



308

309 Figure 15 - Comparison of angle of rotation of brace in clockwise and anticlockwise torsion

310 **Conclusion**

311 Here an experimental test rig and finite element simulation has been developed for the first  
 312 time that mimics the mechanical behaviour of the human torso, with the purpose of

313 facilitating the design of back braces. The test rig and simulation models incorporate a  
314 mechanically equivalent artificial spine with geometries and properties that are comparable to  
315 those found in human tissues. This allows researchers to test different back brace  
316 configurations without having to resort to human testing in the first instance with all the  
317 logistical and ethical issues that those tests necessitate. Another advantage of this novel  
318 design process is that the back braces can be compared quantifiably in a more convenient  
319 manner than in traditional design strategies. It also means that different spine configurations  
320 and deformities, such as scoliosis, can be modelled and tested with different back braces  
321 without causing any discomfort. It is recognised that ultimately, testing on humans is  
322 necessary in order to optimise for factors such as comfort and muscle engagement, but this  
323 new design process should facilitate innovation in this field.

#### 324 ***Acknowledgments***

325 Competing interests: None declared

326 Funding: Lancaster University Engineering Department

327 Ethical approval: Not required

#### 328 ***References***

329 An, N., 2014. *Human spine*. [Online]

330 Available at: <https://grabcad.com/library/human-spine-1>

331 [Accessed 01 October 2018].

332 ANSYS, 2017. Workbench - Mechanical Introduction 18.0.

333 Bayoglu, R. et al., 2019. Twente Spine Model: A thorough investigation of the spinal loads in  
334 a complete and coherent musculoskeletal model of the human spine. *Medical engineering &*  
335 *physics*, Volume 68, pp. 35-45.

336 Bonnaire, R. et al., 2014. Biomechanical analysis and modelling of lumbar belt: parametric  
337 study. *Computer Methods in Biomechanics and Biomedical Engineering*, S1(62-63), p. 17.

338 Carboni, M. & Dal Pozzo, E., 2017. *Integration of muscle forces and gravity loads in a finite*  
339 *element model of the lumbar spine*, s.l.: Master Graduation Thesis, Scuola di Ingegneria  
340 Industriale e dell'Informazione Corso di Laurea Magistrale in Ingegneria Biomedica.

341 Cholewicki, J., McGill, K., Shah, K. R. & Lee, A. S., 2010. The effects of a three-week use  
342 of lumbosacral orthoses on trunk muscle activity and on the muscular response to trunk  
343 perturbations. *BMC Musculoskeletal Disorders*, Volume 11.

344 Cholewicki, J., McGill, S. M. & Norman, R. W., 1995. Comparison of muscle forces and  
345 joint load from an optimization and EMG assisted lumbar spine model: Towards  
346 development of a hybrid approach. *Journal of Biomechanics*, 28(3), pp. 321-331.

347 Cholewicki, J., Reeves, N. P., Everding, V. Q. & Morrisette, D. C., 2007. Lumbosacral  
348 orthoses reduce trunk muscle activity in a postural control task. *Journal of Biomechanics*,  
349 40(8), pp. 1731 - 1736.

350 Dreischarf, M. et al., 2014. Comparison of eight published static finite element models of the  
351 intact lumbar spine: predictive power of models improves when combined together. *Journal*  
352 *of Biomechanics*, 47(8), pp. 1757-1766.

353 Eisinger, D. B., Kumar, R. & Woodrow, R., 1996. Effect of lumbar orthotics on trunk muscle  
354 strength. *American Journal of Physical Medicine and Rehabilitation*, 75(3), pp. 194-197.

355 Fayolle-Minon, I. & Calmels, P., 2008. Effect of wearing a lumbar orthosis on trunk muscles:  
356 Study of the muscle strength after 21 days of use on healthy subjects. *Joint Bone Spine*,  
357 75(1), pp. 58-63.

358 Gómez, F., Lorza, R., Bobadilla, M. & García, R., 2017. Improving the process of adjusting  
359 the parameters of finite element models of healthy human intervertebral discs by the multi-  
360 response surface method. *Materials*, 10(10), pp. 1116-1154.

361 Hawkinson, N. V., 2016. *Back Conditions Treated by Spinal Bracing*. [Online]  
362 Available at: [https://www.spineuniverse.com/treatments/bracing/back-conditions-treated-](https://www.spineuniverse.com/treatments/bracing/back-conditions-treated-spinal-bracing)  
363 [spinal-bracing](https://www.spineuniverse.com/treatments/bracing/back-conditions-treated-spinal-bracing)  
364 Hoy, D. et al., 2014. The global burden of low back pain: estimates from the Global Burden  
365 of Disease 2010 study. *Annals of the Rheumatic Diseases*, 73(6), pp. 968-974.  
366 Hsu, J. D., Michael, J. & Fisk, J., 2008. *AAOS Atlas of orthoses and assistive devices e-book*.  
367 s.l.:Elsevier Health Sciences.  
368 Huynh, K. T., Gibson, I. & Gao, Z., 2012. Development of a Detailed Human Spine Model  
369 with Haptic Interface. *In Haptics Rendering and Applications. InTech*, pp. 165-194.  
370 Ivancic, P. C., Cholewicki, J. & Radebold, A., 2002. Effects of the abdominal belt on muscle-  
371 generated spinal stability and L4/L5 joint compression force. *Ergonomics*, 45(7), pp. 501-  
372 513.  
373 Kawaguchi, Y., Gejo, R., Kanamori, M. & Kimura, T., 2002. Quantitative analysis of the  
374 effect of lumbar orthosis on trunk muscle strength and muscle activity in normal subjects.  
375 *Journal of Orthopaedic Science*, Volume 7, pp. 483-489.  
376 Kurutz, M., 2010. Finite element modelling of human lumbar spine. *Finite Element Analysis*.  
377 *InTech*.  
378 Lariviere, C., Caron, J.-M., Preuss, R. & Mecheri, H., 2014. The effect of different lumbar  
379 belt designs on lumbopelvic rhythm in healthy subjects. *BMC Musculoskeletal Disorders*,  
380 15(307).  
381 Longo, U. G. et al., 2012. Conservative management of patients with an osteoporotic  
382 vertebral fracture: a review of the literature.. *The Journal of Bone and Joint Surgery*, 94(2),  
383 pp. 152-157.

384 Materialise, N., 2018. *Materialise Mimics*. [Online]  
385 Available at: <https://www.materialise.com/en/medical/software/mimics>  
386 [Accessed 01 October 2018].

387 Morl, F. & Bradl, I., 2013. Lumbar posture and muscular activity while sitting during office  
388 work. *Journal of electromyography and kinesiology*, 23(2), pp. 362-368.

389 Office for National Statistics, 2017. *Work-related Musculoskeletal Disorders (WRMSDs)*  
390 *Statistics in Great Britain 2017*, London: Office for National Statistics.

391 Panjabi, M. et al., 1992. Human lumbar vertebrae. Quantitative three-dimensional anatomy.  
392 *Spine*, 17(3), pp. 299-306.

393 Pitzer, M. et al., 2016. A numerical study to determine the effect of ligament stiffness on  
394 kinematics of the lumbar spine during flexion. *BMC Musculoskeletal Disorders*, 17(95).

395 Rohlmann, A. et al., 2006. Determination of trunk muscle forces for flexion and extension by  
396 using a validated finite element model of the lumbar spine and measured in vivo data.  
397 *Journal of Biomechanics*, 39(6), pp. 981-989.

398 Schmidt, H. et al., 2006. Application of a new calibration method for a three-dimensional  
399 finite element model of a human lumbar annulus fibrosus. *Clinical Biomechanics*, 21(4), pp.  
400 337-344.

401 Seo, K., Cho, C. & Hong, S., 2013. Evaluation of the shock absorption properties of rigid  
402 polyurethane and polystyrene foam used in a small transport package. *Packaging, Transport,*  
403 *Storage & Security of Radioactive Material*, 16(2), pp. 145-150.

404 Swamy, A., 2014. Material selection for modeling of intervertebral disc. *Int J Scientific*  
405 *Engineering and Research*, 2(4), pp. 51-53.

406 Ultimaker, 2017. *Technical data sheet ABS*. [Online]  
407 Available at: <http://www.farnell.com/datasheets/2310520.pdf>

408 Wagnac, E. et al., 2011. Calibration of hyperelastic material properties of the human lumbar  
409 intervertebral disc under fast dynamic compressive loads. *J Biomech Eng.*, 133(10), p.  
410 101007.

411 Wang, J. P. et al., 2006. Finite element analysis of the spondylolysis in lumbar spine. *Bio-*  
412 *Medical Materials and Engineering*, 16(5), pp. 301-308.

413 Woolf, A. & Pfleger, B., 2003. Burden of major musculoskeletal conditions. *Bulletin of the*  
414 *World Health Organization*, Volume 81, pp. 646-656.

415 Yamamoto, I., Panjabi, M., Crisco, T. & Oxland, T., 1989. Three-dimensional movements of  
416 the whole lumbar spine and lumbosacral joint. *Spine*, 14(11), pp. 1256-1260.

417